TU Delft

Delft University of Technology

Refraction-Corrected Transcranial Ultrasound Imaging through the Human Temporal Window using a Single Probe

Mozaffarzadeh, M.; Verschuur, D.J.; Verweij, M.D.; Daeichin, V.; de Jong, N.; Renaud, G.G.J.

DOI
10.1109/TUFFC.2022.3148121

Publication date
2022

Document Version
Final published version

Published in
IEEE Transactions on Ultrasonics, Ferroelectrics and Frequency Control

Citation (APA)
Mozaffarzadeh, M., Verschuur, D. J., Verweij, M. D., Daeichin, V., de Jong, N., & Renaud, G. G. J. (2022). Refraction-Corrected Transcranial Ultrasound Imaging through the Human Temporal Window using a Single Probe. *IEEE Transactions on Ultrasonics, Ferroelectrics and Frequency Control*, *69*(4), 1191-1203. https://doi.org/10.1109/TUFFC.2022.3148121

Important note
To cite this publication, please use the final published version (if applicable).
Please check the document version above.

Copyright
Other than for strictly personal use, it is not permitted to download, forward or distribute the text or part of it, without the consent of the author(s) and/or copyright holder(s), unless the work is under an open content license such as Creative Commons.

Takedown policy
Please contact us and provide details if you believe this document breaches copyrights.
We will remove access to the work immediately and investigate your claim.

This work is downloaded from Delft University of Technology.
For technical reasons the number of authors shown on this cover page is limited to a maximum of 10.

Green Open Access added to TU Delft Institutional Repository

'You share, we take care!' - Taverne project

https://www.openaccess.nl/en/you-share-we-take-care

Otherwise as indicated in the copyright section: the publisher is the copyright holder of this work and the author uses the Dutch legislation to make this work public.

Refraction-Corrected Transcranial Ultrasound Imaging Through the Human Temporal Window Using a Single Probe

Moein Mozaffarzadeh, *Graduate Student Member, IEEE*, Eric Verschuur, Martin D. Verweij, *Member, IEEE*, Verya Daeichin, *Member, IEEE*, Nico de Jong, *Member, IEEE*, and Guillaume Renaud

***Abstract*— Transcranial ultrasound imaging (TUI) is a diagnostic modality with numerous applications, but unfortunately, it is hindered by phase aberration caused by the skull. In this article, we propose to reconstruct a transcranial B-mode image with a refraction-corrected synthetic aperture imaging (SAI) scheme. First, the compressional sound velocity of the aberrator (i.e., the skull) is estimated using the bidirectional headwave technique. The medium is described with four layers (i.e., lens, water, skull, and water), and a fast marching method calculates the travel times between individual array elements and image pixels. Finally, a delay-and-sum algorithm is used for image reconstruction with coherent compounding. The point spread function (PSF) in a wire phantom image and reconstructed with the conventional technique (using a constant sound speed throughout the medium), and the proposed method was quantified with numerical synthetic data and experiments with a bone-mimicking plate and a human skull, compared with the PSF achieved in a ground truth image of the medium without the aberrator (i.e., the bone plate or skull). A phased-array transducer (P4-1, ATL/Philips, 2.5 MHz, 96 elements, pitch = 0.295 mm) was used for the experiments. The results with the synthetic signals, the bone-mimicking plate, and the skull indicated that the proposed method reconstructs the scatterers with an average lateral/axial localization error of 0.06/0.14 mm, 0.11/0.13 mm, and 1.0/0.32 mm, respectively. With the human skull, an average contrast ratio (CR) and full-width-half-maximum (FWHM) of 37.1 dB and 1.75 mm were obtained with the proposed approach, respectively. This corresponds to an improvement of CR and FWHM by 7.1 dB and 36% compared with the conventional method, respectively. These numbers were 12.7 dB and 41% with the bone-mimicking plate.**

***Index Terms*— Adaptive beamforming, head waves, phase aberration correction, temporal bone, transcranial ultrasound imaging (TUI).**

I. Introduction

TRANSCRANIAL ultrasound imaging (TUI) is a diagnostic modality with numerous applications, such as stroke diagnosis [1]–[6], detection of vasospasm after subarachnoid hemorrhage (most often caused by head trauma) [7], [8], microemboli [9], [10], and endonasal trans-sphenoidal surgery [11]–[13]. A growing number of recent ultrasound technologies are being applied to the brain, in particular, ultrasound localization microscopy [14]–[16], functional ultrasound imaging [17], [18], and perfusion imaging with ultrasound contrast agents [19]. At present, it is safe, relatively inexpensive, and available in hospitals and emergency medicine services (EMS) [6], [20]–[22]. Despite its advantages, TUI is still hindered by the low image quality caused by the strong aberration and scattering [23], multiple reflections caused by the skull [24], [25], and mode conversion [26].

TUI is often performed through the temporal window, which enables imaging of the arteries of the circle of Willis. The temporal bone is the thinnest part of the skull that gives direct access to the brain, and unlike most parts of the skull, the squamous part of the temporal bone often consists of a single layer of cortical bone. Its thickness and mass density vary from 1.5 to 4.4 mm [27]–[30] and 1700 to 2000 kg/m^3, respectively [29]. The cortical bone tissue of the temporal bone was found to have anisotropic elasticity [29]. The compressional wave velocity (Vc) was 3520 m/s in the direction normal to the surface of the skull. Vc varied between 3590 and 4000 m/s in different propagation directions within the plane of the temporal bone [29]. Moreover, a relatively lower attenuation through the temporal bone was reported (one-way attenuation

Manuscript received September 21, 2021; accepted January 28, 2022. Date of publication January 31, 2022; date of current version March 28, 2022. This work was supported in part by the Netherlands Organisation for Scientific Research (NWO)/the Netherlands Organisation for Health Research and Development (ZonMw) and in part by the Department of Biotechnology (Government of India) through the Program Medical Devices for Affordable Health (MDAH) as Project Imaging Needles under Grant 116310008. *(Corresponding author: Moein Mozaffarzadeh.)*

Moein Mozaffarzadeh, Verya Daeichin, and Guillaume Renaud are with the Laboratory of Medical Imaging, Department of Imaging Physics, Delft University of Technology, 2628 CD Delft, The Netherlands (e-mail: m.mozaffarzadeh@tudelft.nl).

Eric Verschuur is with the Section of Computational Imaging, Department of Imaging Physics, Delft University of Technology, 2628 CD Delft, The Netherlands.

Martin D. Verweij and Nico de Jong are with the Laboratory of Medical Imaging, Department of Imaging Physics, Delft University of Technology, 2628 CD Delft, The Netherlands, and also with the Department Biomedical Engineering, Thoraxcenter, Erasmus Medical Center, 3015 GD Rotterdam, The Netherlands.

This article has supplementary downloadable material available at https://doi.org/10.1109/TUFFC.2022.3148121, provided by the authors.

Digital Object Identifier 10.1109/TUFFC.2022.3148121

1525-8955 © 2022 IEEE. Personal use is permitted, but republication/redistribution requires IEEE permission.
See https://www.ieee.org/publications/rights/index.html for more information.

Authorized licensed use limited to: TU Delft Library. Downloaded on April 25,2022 at 06:57:05 UTC from IEEE Xplore. Restrictions apply.

at normal incidence from 13 to 22 dB/cm/MHz [31]) compared with other parts of the skull that can be as thick as 1 cm [23]. In the presence of a diploe, i.e., a layer of highly porous trabecular bone sandwiched between inner and outer tables made of dense cortical bone, the attenuation is largely determined by the thickness of the diploe. The one-way attenuation through the skull can exceed 25 dB/cm/MHz for a diploe thickness of 6 mm [23]. In contrast, a temporal bone made of a single layer of cortical bone (absence of diploe) produces a one-way attenuation at normal incidence close to 13 dB/cm/MHz [31]. While this makes the temporal bone a suitable window to image through, temporal window failure (TWF) is present in 8%–20% of people [32]. There are several parameters affecting TWF: age, sex, temporal bone thickness, pneumatization (presence of cancellous bone or air sandwiched between two layers of cortical bone instead of one single layer of cortical bone), and soft tissue thickness [28], [30]. The larger the thickness of the temporal bone, the higher the chance of failure; the probability of TWF was 93.5% for a heterogeneous temporal bone with a thickness larger than 2.7 mm [30]. The most important cause of TWF is pneumatization with an odds ratio of 7.9 [27]. While solely reduction of the central frequency of the probe might not be helpful [33], contrast agents significantly increase the backscattered signals power and seem to reduce the chance of TWF [2], [34], [35]; depending on the concentration of the contrast agent, the average signal-to-noise enhancement could be about 12 ± 5.4 dB [34].

Since the pioneering work by Smith *et al.* [36], [37], different methods and techniques have been developed to compensate the phase aberration caused by the skull [38]. However, these techniques have had moderate success in diagnostic ultrasound imaging (the discussion section includes a review of earlier methods). Most approaches use the near-field phase-screen aberration model which models the skull as an infinitesimally thin aberrating layer at the surface of the transducer [39]–[41]. A limitation of this approach is that the effects of refraction and irregular skull thickness (or geometry) are not correctly modeled and, therefore, the correction is only valid for a certain region called the isoplanatic patch [24], [41], [42], [42]–[45]; the use of multiple isoplanatic patches enables aberration correction throughout a larger region of interest [33], [46], [47]. This strategy was used for two dimensional (2-D) [24], [42] and 3-D TUI [46], [48], [49]. More recently, approaches that model refraction through the true geometry and thickness of the skull have been proposed; however, the method requires estimates of the thickness and wave speed in the skull at multiple positions with dedicated ultrasound measurements prior to image reconstruction [50]–[52]. Another family of methods relies on a CT or MRI scan of the skull to determine its geometry and knowledge or assumption of wave speed in bone, prior to TUI [53]–[56].

As a result of the large acoustic impedance mismatch between bone and soft tissues, the near and far surfaces of the temporal bone appear as bright interfaces in the ultrasound image, and their detection and segmentation is, therefore, rather easy. This study capitalizes on this to attempt a new type of aberration correction, aiming to improve transcranial ultrasound B-mode images. The novelty of our approach lies in the fact that it corrects for the true position and the true geometry of the bone layer. This means that the tilt and the distance between the temporal bone and the probe are taken into account, and the outer and inner surfaces of the temporal bone are described as nonplanar and nonparallel surfaces. Moreover, our approach estimates the wave speed in the bone layer prior to imaging, all with a single ultrasound array transducer. As a result, delay-and-sum image reconstruction provides improved image quality because the travel times through the layered medium are accurately calculated at each image pixel. A synthetic aperture imaging (SAI) scheme is used as the transmission of spherical wave fronts facilitates the modeling of refraction (necessary for an accurate phase correction) and provides dynamic focusing in transmission [57]. As explained in [58], modeling the wave propagation through the skull and considering a bone layer with a finite irregular thickness enable the calculation of a unique set of forward and backward travel times, at each pixel, for each transmit beam and for each array element (in receive). As a consequence, we expect our approach to overcome the limitations of near-field phase-screen methods, in particular, because the concept of isoplanatic patch does not exist in our approach.

The compressional wave speed is first estimated in the temporal bone with the bidirectional headwave method [59]–[61]. Next, sound speed maps (SSMs) are generated with adaptive beamforming [62], [63]. Travel times are calculated with the fast marching technique (FMT) [64], [65]. The point spread function (PSF) is evaluated with numerical simulations and experiments, before and after correction, and compared with a ground truth image.

II. Materials and Methods

The proposed approach is briefly presented in Fig. 1. Image reconstruction starts with a primary SSM. After each segmentation step, the SSM is updated and new reconstruction is performed. Note that the terms far and near are in relation to the probe throughout this article.

A. Compressional Wave Speed Estimation in the Aberrator

The bidirectional headwave method was used before to estimate the compressional wave speed of cortical bone [59]–[61]. This method works based on the propagation of the head wave (the first arriving signal) along a planar interface and is briefly explained as follows.

1) The first element of the ultrasound array transmits and other elements receive.
2) The head wave is extracted by defining a range for the compressional wave speed of the aberrator.
3) A 2-D fast Fourier transform (FFT) is applied on the extracted head wave to convert the temporal-spatial data into the frequency–wavenumber (f-k) domain [66].
4) The slope of the line fit on the high intensity region multiplied by 2π results in a compressional wave speed, V_1.

Authorized licensed use limited to: TU Delft Library. Downloaded on April 25,2022 at 06:57:05 UTC from IEEE Xplore. Restrictions apply.

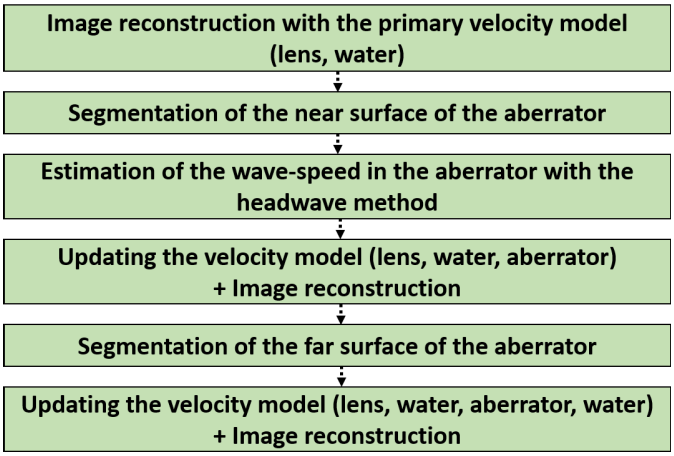

Fig. 1. Flowchart of the proposed image reconstruction method.

5) V_1 is biased if the aberrator is not parallel to the probe [61]. To compensate for this, the last steps should be repeated, but the last element of the arrays should transmit and other elements receive in the step 1. This results in a second compressional wave speed, V_2.
6) The compressional sound velocity of the aberrator is finally calculated by

$$(2V_1V_2\cos(\alpha))/(V_1+V_2) \tag{1}$$

where α is the angle between the surface of the probe and the aberrator [67]. The method is accurate if the thickness of the aberrator is larger than the wavelength and can also be used to estimate the compressional sound velocity in the lens of the probe. As the head wave is not dispersive, the fit line at step 4 should pass (0, 0) in the f-k domain. The wave speed estimated with the headwave technique in this study is the compressional sound speed in the temporal bone in the lateral direction (relative to the ultrasound probe).

B. Adaptive Beamforming

The formula of delay-and-sum (DAS) beamformer is [57], [67] as follows:

$$I(p)=\sum_{i=1}^{M}\sum_{j=1}^{N}\mathrm{RF}(t=t_T(i,p)+t_R(j,p),i,j)\times W(P,i,j) \tag{2}$$

where I is the output of the beamformer at pixel p; M and N are the number of transmission and reception events, respectively; RF is the recorded data; t_T and t_R are the transmit and receive arrival times, respectively; and $W(P,i,j)$ is a weight calculated for pixel p. In this article, this weight is based on the far-field directivity of the elements of the array [68], [69].

Traditionally, a constant wave speed is assumed throughout the medium during image reconstruction; the term "conventional" in this manuscript represents results generated with a constant wave speed. However, in transcranial scenario, this imposes inaccuracies in the calculated arrival times for each pixel of the image [67], [70], [71]. To accurately reconstruct the images, the refraction caused by the skull (directly affecting the arrival times used for beamforming) should be taken into account. To this end, the FMT was used. FMT solves the Eikonal equation and calculates the arrival times given SSMs [64], [65]. The "scikit-fmm" Python toolbox was used to employ the FMT; available in "https://pypi.org/project/scikit-fmm/." We used three stages of adaptive beamforming to reconstruct phase-compensated images: one to segment the near surface of the aberrator, one to segment the far surface, and one to reconstruct the region of interest (usually at depths more than 15 mm). For segmentation, a technique based on Dijkstra's algorithm was used [72], [73]. The segmentation algorithm seeks the shortest path that follows the interface with the highest intensity in the ultrasound image, by maximizing a merit, here, the sum of the pixel values along the path.

Once the near/far surface of the aberrator is segmented, the sound speed of the aberrator/soft tissue is assigned to the depths higher than the near/far surface and passed to FMT.

C. Numerical Study

The k-Wave MATLAB toolbox was used to evaluate the proposed method in a 2-D lossless medium, ignoring shear wave propagation [74]. Seven point scatterers were placed in different lateral and axial distances [see Fig. 2(a)]. The speed of sound in lens, skull, and soft tissue was 1000, 3200, and 1600 m/s, respectively. The mass density of the soft tissue/lens and skull was 1000 and 1900 kg/m^3, respectively. The grid and time step size were 20 μm and 4 ns, respectively, to avoid numerical dispersion and maintain the stability and accuracy of the simulation. The near surface of the skull was planar and parallel to the probe, but the far surface was modeled irregular to evaluate the performance of our method under a severe condition. The minimum and maximum thickness of the skull was 2.1 and 4.1 mm, respectively. After the lens layer, 2.1 mm in depth was modeled as skin. The properties of a P4-1 phased-array transducer (ATL/Philips, 2.5 MHz, 96 elements, pitch = 0.295 mm) and the SAI sequence were used to assemble the numerical signals [57]. To have a ground truth image, the same model [Fig. 2(a)], but without the aberrator, was simulated.

D. Experimental Setup

We configured two experimental setups: one with a 4.23 $\pm$ 0.01 mm-thick (measured with a caliper) bone-mimicking plate (Sawbones, Pacific Research Laboratory, Inc., Vashon, WA, USA) [see Fig. 2(b)] and one with a sagittally cut human skull [see Fig. 2(c)]. The Sawbones plate is transverse isotropic. We used the plane perpendicular to the material fibril orientation to have isotropic compressional wave speed. The human skull (Skulls Unlimited International Inc., Oklahoma, OK, USA) was carefully prepared with the use of dermestid beetles. It was degreased and whitened using a chemical process (peroxided) to ensure an attractive and sanitary trophy or display piece. Before experiments, the skulls were degassed at 80 mBar for 48 h.

Authorized licensed use limited to: TU Delft Library. Downloaded on April 25,2022 at 06:57:05 UTC from IEEE Xplore. Restrictions apply.

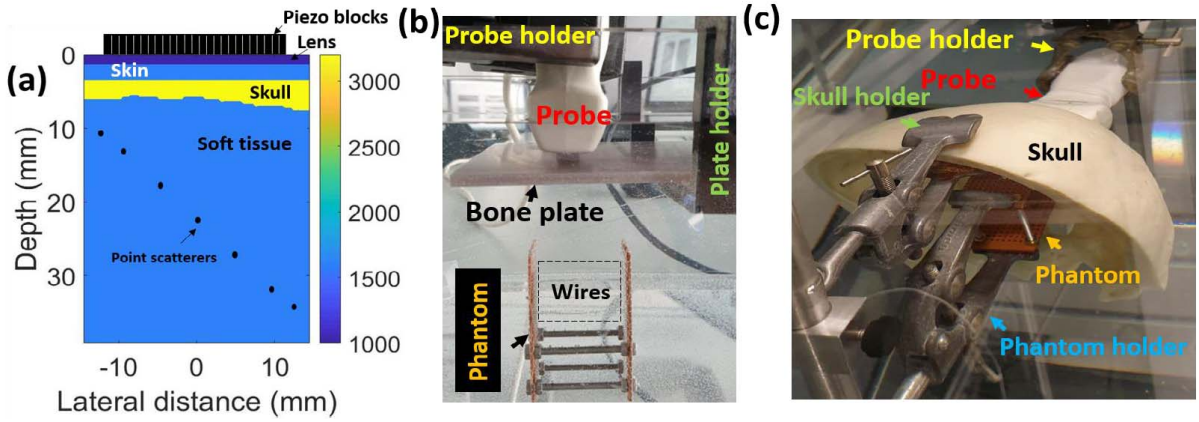

Fig. 2. (a) Numerical model used in *k*-Wave. (b) and (c) Experimental setup used to image the wire phantom through a bone plate (Sawbones, Pacific Research Laboratory, Inc., Vashon, WA, USA) and human skull, respectively. The imaging plane is perpendicular to the wires in (b) and (c) and perpendicular to the material fibril orientation of the Sawbones plate in (b).

A phantom including multiple wires (50-μm diameter) was used. The imaging plane of the one dimensional (1-D) probe was perpendicular to the wires. Therefore, the wires are expected to mimic point scatterers considering their diameter (about one-tenth of the wavelength at the central frequency). To have a ground truth measurement, the probe was moved against the phantom with a XYZ system, the skull was carefully removed from the setup, and finally the probe was moved back to its first place; the rest of the components were fixed. All the experiments were conducted with a phased-array transducer (P4-1, ATL/Philips, 2.5 MHz, 96 elements, pitch = 0.295 mm) connected to a Verasonics Vantage 256 system. The wire phantom was placed at a depth of 3–4 cm, which corresponds to the depth of the nearest middle cerebral artery.

E. Evaluation Metrics

To evaluate the reconstructed images, we compared the coordinates of the scatterers, full-width-half-maximum (FWHM), contrast ratio (CR), and absolute amplitude of the main lobe of the PSF (AAM). The CR is defined as the ratio between the max brightness of scatterers to the mean brightness of background noise (indicated later in the figures) and is reported in decibel. The brightness is calculated from the envelope of the beamformed RF data, before normalization and log compression. It should be noted that the image reconstructed by the conventional method in the followings represents a noncorrected image in our study.

III. Results

A. Numerical Results

The numerical space-time domain data and the corresponding f-k representation used to apply the bidirectional head-wave method are presented in Fig. 3. The head wave (the first arriving signal) appears as a planar wavefront because the near surface of the aberrator is planar [see Fig. 2(a)]. The estimated wave speeds in Fig. 3(c) and (d) with an $\alpha = 0$ (parallel near surface) result in a sound speed of 3200.5 m/s [following (2)].

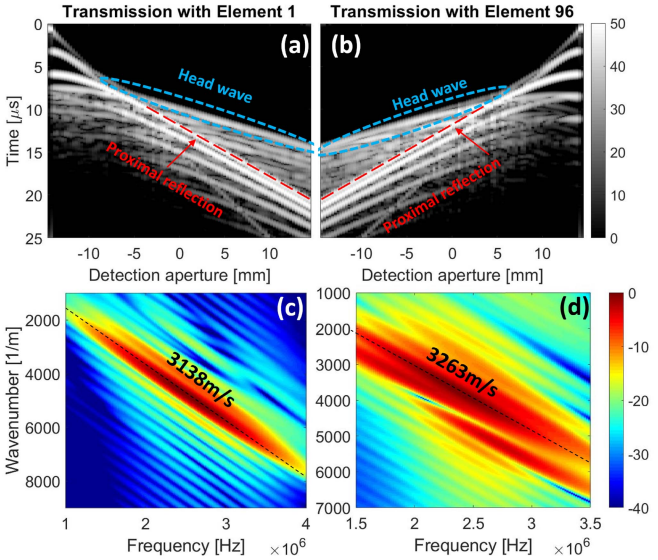

Fig. 3. (a) and (b) Numerical space-time domain data and (c) and (d) corresponding *f-k* representation, respectively.

This estimation has a small error of 0.5 m/s (the true sound speed is 3200 m/s).

Fig. 4 shows the procedure taken to extract the SSM of the aberrator (see Section II-B). Taking the sound speed of the lens layer into account [Fig. 4(a)] helps with accurately reconstructing the reflections of the lens layer and near surface [see Fig. 4(b)]. Once the SSM gets updated based on the segmented near surface [see Fig. 4(c)], the far surface is also accurately reconstructed and segmented [see Fig. 4(d)]. Fig. 4(e) shows the finalized SSM closely following the actual model [the dashed line shows the far surface of the actual model presented in Fig. 2(a)].

The scatterers are better detected with the proposed method [comparing Fig. 5(c) and (b)] because wave physics in the layered medium is accurately described. This also results in a lower level of sidelobes and clutter; to have a fair comparison, compare Fig. 5(e) with (d), since these images

Authorized licensed use limited to: TU Delft Library. Downloaded on April 25,2022 at 06:57:05 UTC from IEEE Xplore. Restrictions apply.

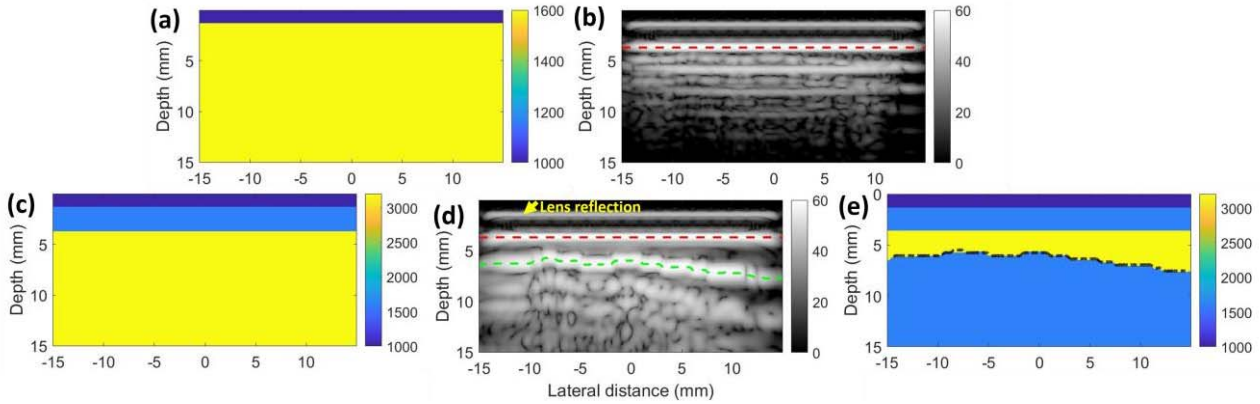

Fig. 4. (a) and (b) SSM and corresponding reconstructed image taking the lens into account, respectively. (c) and (d) SSM and corresponding reconstructed image taking the sound speed of the aberrator into account, respectively. (e) SSM used to compensate the phase aberration and image the point scatterers; the dashed black line shows the far surface of the actual model [see Fig. 2(a)]. The red and green dashed lines indicate the near and far surfaces of the aberrator, respectively.

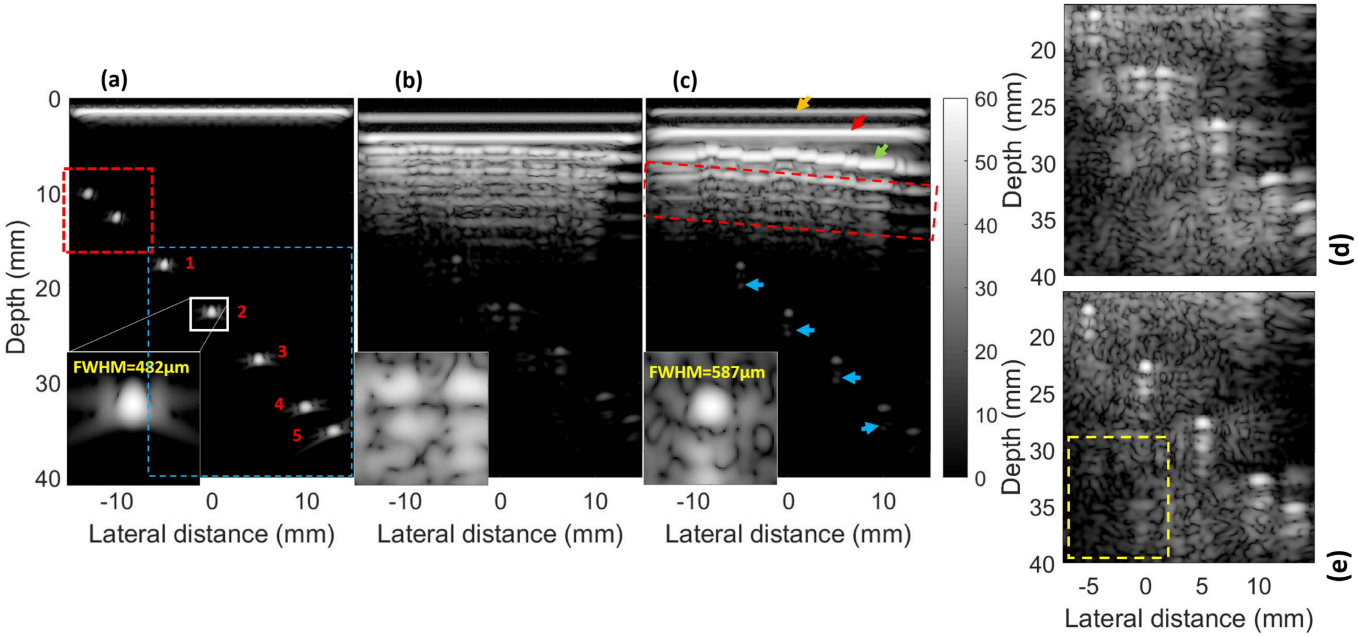

Fig. 5. Reconstructed images (a) without and (b) and (c) with the aberrator in the numerical model. The red dashed rectangle in (c) shows the effects of multiple reflections caused by the aberrator. The red dashed square in (a) shows the two targets that are not visible in (c) due to the effects of multiple reflections caused by the aberrator. The zoomed version of the figures shows −2 to 2 mm and 20 to −24 mm in the lateral and depth directions, respectively; these images are normalized to the maximum intensity after a depth of 15 mm. This is also the case in (d) and (e) which present the area indicated by the blue dashed box shown in (a). The numbers in (a) and the yellow dashed box in (e) are used to refer scatterers for quantitative evaluation and calculate CR in Table I, respectively. The orange, red, and green arrows show the reflections of the lens, near, and far surfaces, respectively.

were normalized to their local maximum but not the global one. Multiple reflections within the aberrator create significant artifacts at shallow depth [see Fig. 5(c) (red dashed rectangle)]. This causes the first two scatterers to disappear [see the red dashed square in Fig. 5(a)]. The artifacts behind the scatterers indicated by the blue arrows are also due to multiple reflections caused by the aberrator.

As indicated in Table I, the proposed method reconstructs the scatterers with an average lateral and axial localization error of about 0.06 and 0.14 mm, compared with the ground truth, respectively. For the conventional method, these quantities are 1 and 0.96 mm, respectively. The proposed method in average improves the CR by 4.4 dB, the FWHM by 22%, and the AAM by 107% (+6.3 dB), compared with the conventional method. Refer to Table S1 in the supplementary material for details.

B. Experimental Results

1) Bone-Mimicking Plate: The space-time domain data and the corresponding f-k representation of the experiment conducted with the Sawbones plate are presented in Fig. 6. The sound speeds estimated in Fig. 6(c) and (d) with an α of about 3.3° result in a sound speed of 3058 m/s. A thickness of 4.2 mm was obtained with the proposed approach (0.7% error),

Authorized licensed use limited to: TU Delft Library. Downloaded on April 25,2022 at 06:57:05 UTC from IEEE Xplore. Restrictions apply.

TABLE I
QUANTITATIVE EVALUATION OF THE NUMERICAL AND EXPERIMENTAL IMAGES

	Metric / Method	Axial/lateral Localization error (mm)	FWHM (mm)	Contrast ratio (dB)
Simulation	Conventional	[1.0, 0.96]	1.00	35.5
	Proposed	[0.06, 0.14]	0.78	39.9
Sawbones Plate	Conventional	[0.7, 1.9]	1.80	23.1
	Proposed	[0.11, 0.13]	1.06	35.8
Human skull	Conventional	[1.45, 1.17]	2.72	30.0
	Proposed	[1, 0.32]	1.75	37.1

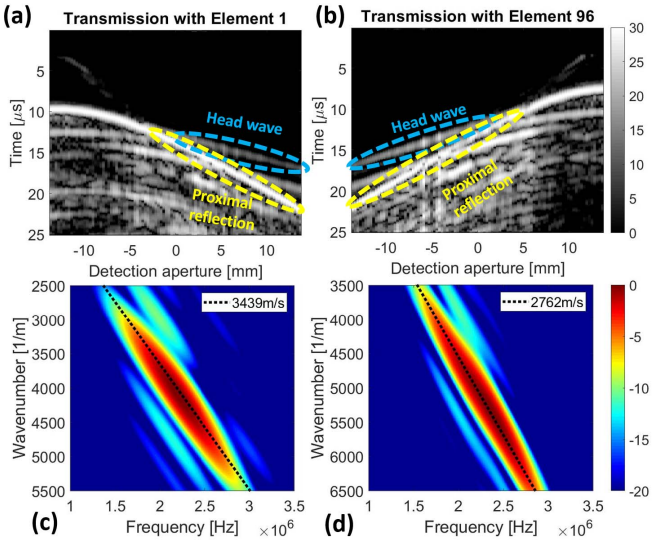

Fig. 6. (a) and (b) Experimental space-time domain data and (c) and (d) corresponding representation after 2-D Fourier transform of the space-time domain data. The Sawbones plate was used as the aberrator.

while the conventional method underestimates the thickness for about 2 mm (comparing Fig. 7(b) and (c)]. The blue arrows [see Fig. 7(c)] indicate the trailing clutter resulting from multiple reflections caused by the Sawbones plate [75]. The same procedure shown in Fig. 4 is used to extract the SSM of the Sawbones plate, but results are not provided.

The proposed method reconstructs the scatterers (i.e., wires) with an average lateral and axial localization error 0.11 and 0.13 mm, compared with the ground truth, respectively (see Table I). For the conventional method, these quantities are 0.7 and 1.9 mm, respectively. The proposed method in average improves the CR by 12.6 dB, the FWHM by 45%, and AAM by 167% (+8.5 dB), compared with the conventional method. Refer to Table S2 in the supplementary material for details.

2) Human Skull: The space-time domain data and the corresponding f-k representation of the experimental data used to apply the bidirectional headwave method are presented in Fig. 8. A sound speed of 3500 m/s is obtained considering $\boldsymbol{V_1}$ [Fig. 8(c)], $\boldsymbol{V_2}$ [Fig. 8(d)], and $\boldsymbol{\alpha}$ of 3° [see Fig. 9(c)]. We found a compressional wave speed in temporal cortical bone in agreement with [29]. Although the elasticity of temporal cortical bone is anisotropic [29], we assume isotropic elasticity in this work.

The proposed method enhances the visibility of the wires [comparing Fig. 9(c) and (b)] because the wave physics in the layered medium is accurately described. The mean thickness of cortical bone was estimated 1.3 mm; there is no information available on the true thickness of the skull within the imaging plane. The clutter shown by the yellow dashed box is caused by the multiple reflections of the backscattered wave from the far surface. The level of the clutter behind the wires in Fig. 9(c) (see the blue arrows), caused by multiple reflections, looks higher since the images are normalized to their global maximum. Fig. 9(d) and (e) is normalized to their local maximum and can be used for a fair visual comparison. The level of background noise is higher in Fig. 9(d), compared with Fig. 9(e), due to the distribution of energy to different pixels, which is mainly caused by the refraction induced by the skull. The proposed method reconstructs the scatterers with an average lateral and axial localization error of about 1 and 0.32 mm, compared with the ground truth, respectively (see Table I). For the conventional method, these quantities are 1.45 and 1.17 mm, respectively. The proposed method in average improves the CR by 7.1 dB, FWHM by 36%, and AAM by 130% (+7.2 dB), compared with the conventional method. Refer to Table S3 in the supplementary material for details.

IV. DISCUSSION

A. Comparison With Previous Relevant Works

1) Estimating the Compressional Wave Speed and Thickness of the Aberrator: The periodicity of the frequency spectrum of the signals reflected within a bone layer was used in a model to determine the wave speed in *ex vivo* human skulls, assuming a known bone thickness [76]. Different strategies using a single focused transducer and a phased array were proposed in [77] and [78] for independent measurement of compressional wave velocity and thickness of the cortical bone. The technique proposed by Wydra *et al.* [77] consists in varying the focal depth of a focused beam and searching for maximum reflected amplitude, and it was originally introduced for acoustical microscopy (see in [89]). The method is essentially a 1-D approach and requires: 1) clearly distinct reflected echoes from the near and far surfaces of the skull and 2) a locally flat skull surface and parallel to the probe. For a flat non-porous aberrator with a thickness of 7.21 mm, their approach estimated a thickness of 7.55 mm (4.9% error) with a phased-array transducer. With a thinner aberrator (4.23-mm-thick Sawbone plate used in this study) and a nearly equal ultrasound frequency (2.5 versus 2.25 MHz), and our approach estimated the plate thickness with an error of 0.7%. Tilted or non-flat surfaces reduce the accuracy of thickness and sound speed estimation with the technique proposed by Wydra *et al.* [77]. This method was improved by Postert *et al.* [90] by using a higher frequency (5 versus 2.25 MHz) and by considering the effective aperture during measurements, but was still limited to plate-shape aberrators with constant thickness and parallel to the transducer array.

Authorized licensed use limited to: TU Delft Library. Downloaded on April 25,2022 at 06:57:05 UTC from IEEE Xplore. Restrictions apply.

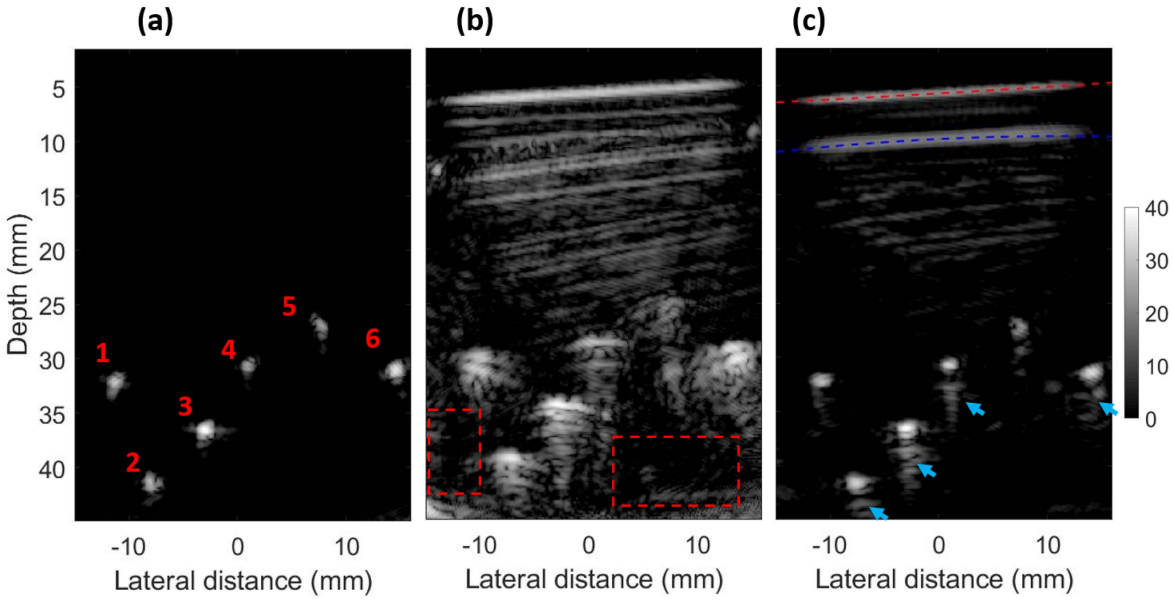

Fig. 7. Reconstructed images (a) without and (b) and (c) with the Sawbones plate in front of the probe. The red and blue dashed lines show the reflections of near and far surfaces, respectively. The blue arrows show the effects of multiple reflections caused by the aberrator (i.e., Sawbones plate). The numbers in (a) and the red dashed boxes in (b) are used to point out the scatterers for quantitative evaluation and calculate CR in error! Reference source not found.

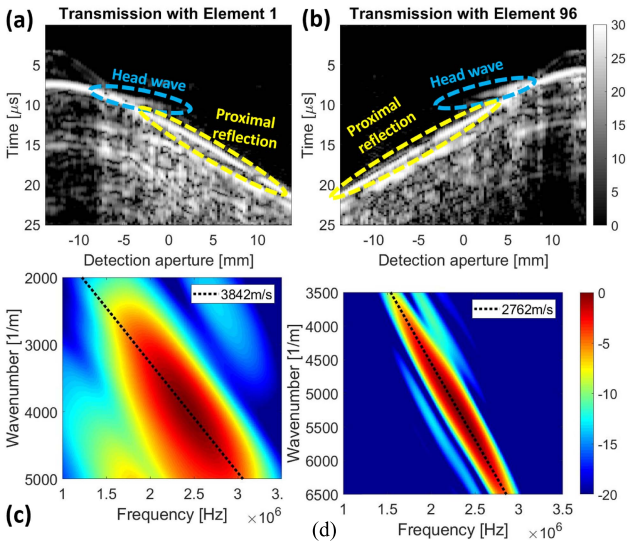

Fig. 8. (a) and (b) Experimental space-time domain data and (c) and (d) corresponding representation after 2-D Fourier transform of the space-time domain data. The skull was used as the aberrator.

An autofocus approach combined with ultrasound imaging was also proposed to estimate the wave speed and thickness of the cortex of long bones [67], [79]. The rationale of this approach is simple: a reconstructed ultrasound image shows optimal quality (intensity and sharpness) if the wave speed model used during image reconstruction is correct. Therefore, looking for the value that maximizes image intensity and sharpness provides an estimate of the wave speed.

In this work, we chose to use the bidirectional headwave technique because it provides an independent estimate of the compressional wave speed in the aberrator and the signal processing is straightforward if the near surface of the aberrator is locally sufficiently planar. In addition, the same array transducer can be used for wave speed estimation and imaging.

2) Phase Aberration Compensation: Other researchers proposed different strategies to tackle phase aberration (or refraction). Deng *et al.* [80] used thickness resonance frequencies in the skull for phase shift calculation, which might enable adaptive focusing during high-intensity transcranial ultrasound treatments. Clement *et al.* [81] and Lucht *et al.* [82] reported mode converted shear waves for focusing the ultrasound wave in brain. Shear wave velocity in the skull is lower than its compressional wave velocity, which results in a better impedance match with soft tissues and less refraction; at 0.74 MHz, mode converted shear wave has a smaller but exploitable amplitude compared with the compressional wave (between 35% and 55% of the peak of the compressional wave). However, in a later study, White *et al.* [83] reported that the shear attenuation of skull can be 2–3 times higher (in dB/cm) than the compressional attenuation (a longitudinal and shear attenuation coefficient of 6.1 and 18.5 dB/cm, at a frequency of 0.84 MHz, respectively), which overshadows the relatively better impedance match of the shear wave. Yousefi *et al.* [84] also reported that transcranial shear wave imaging causes equal distortion and worsens lateral resolution compared with using compressional waves for imaging.

In [16], [43]–[45], [85], and [86], the near-field phase screen aberrator model [39]–[41] was used to extract the profile of the aberrator. This model assumes an infinitely thin aberrating layer attached to the surface of the probe [43] and only works in a limited area (called isoplanatic patch) around the region of interest [41], [43], [87]. Correction of multiple isoplanatic patches was achieved in [33] and [46], but with two 2-D matrix arrays placed on the opposing sides of the skull, one on each of the temporal bones; transmission from

Authorized licensed use limited to: TU Delft Library. Downloaded on April 25,2022 at 06:57:05 UTC from IEEE Xplore. Restrictions apply.

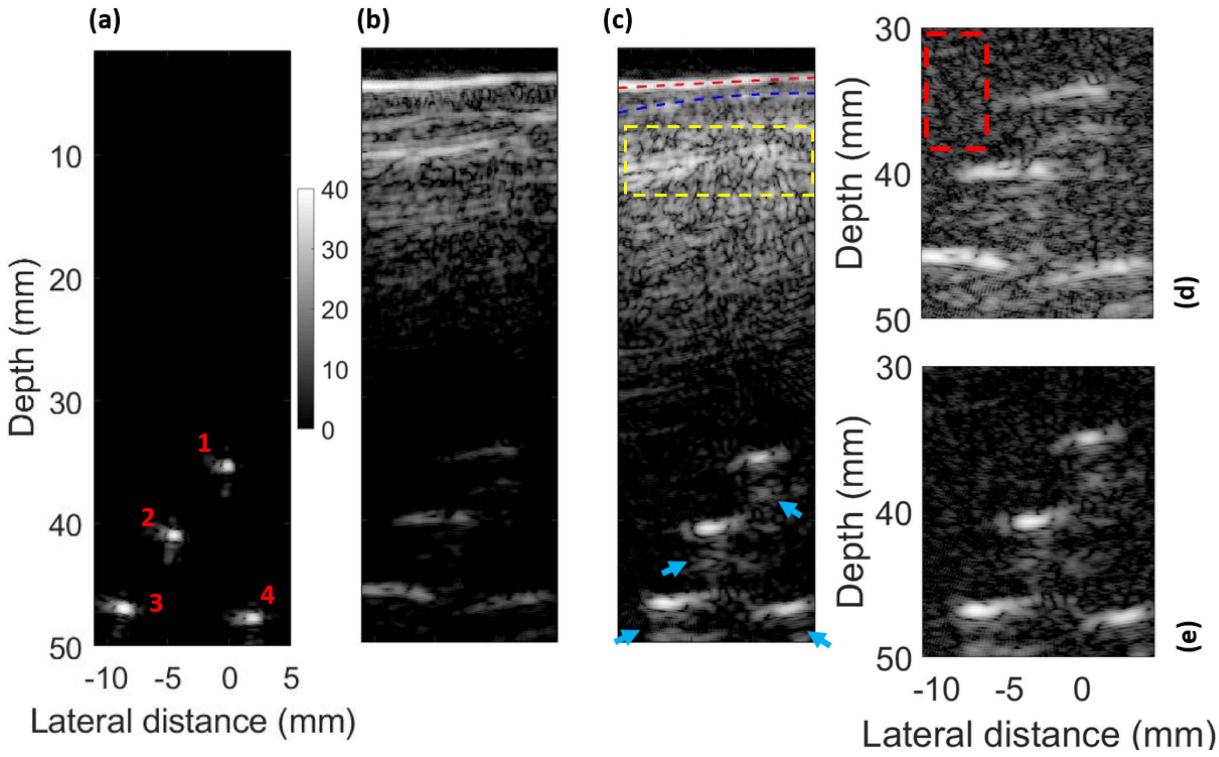

Fig. 9. Reconstructed images (a) without and (b) and (c) with the skull in front of the probe. (d) and (e) Zoomed version of (b) and (c), respectively; these figures are normalized and log compressed to the local maximum. The red and blue dashed lines in (c) show the near and far surfaces of the skull, respectively. The yellow dashed box indicates the effects of multiple reflections. The numbers in (a) and the red dashed box in (d) were used to point out the scatterers for quantitative evaluation and calculate background noise in Table I, respectively.

one side and reception in other side provided unique delay maps which could be used for phase compensation in the entire 3-D volume. The effectiveness of this method was evaluated in healthy volunteers; it improved the detection of large cerebral arteries (more arteries of the circle of Willis visualized and detected volume of arteries increased by 34%) [47], and the image brightness was improved by 24% [33]. Our approach increased the AAM by 130% in experiments with water in an *ex vivo* skull. Studies in [33] were *in vivo* and thus had scattering from brain tissue. The idea of using two array transducers facing each other and sharing the same imaging plane (an imaging transducer and a calibration transducer), one on each of the temporal bones, was also proposed by Vignon *et al.* [24]. Their approach relies on the measurement of the impulse response between all pairs of individual elements of the two array transducers, in order to estimate a spatiotemporal inverse filter. The −6-dB width of the focal spot was improved by 32% (from 4.9 to 3.3 mm), the lateral shift of the focal spot by 63% (from 1.1 to 0.4 mm), and the contrast loss by 65% (from 15.1 to 5.3 dB), on average. The approach proposed by Vignon *et al.* [24] achieves improvements close to our approach (see Table I), using a more complicated setup than ours with two probes. Also, in order to migrate the spatiotemporal inverse filter (measured between the two array transducers) inside the skull, one side of the skull was assumed infinitely thin and located close to the calibration transducer array. As a result, optimal focusing with the imaging transducer was limited to a region, at rather large depth (for the imaging transducer) close to the part of the skull in contact with the calibration transducer, and at lateral positions where the skull was sufficiently flat to enable close contact with the calibration transducer. Prior knowledge on the compressional sound speed or thickness of skull [53], [58], [76], [88], [89] and correction based on CT scans [53]–[55] are also impractical on-site as these parameters vary in person [23], [25], [29], [51], [52], [90], [93] and EMS are not always equipped with CT scanners.

Similar studies to our phase correction technique were reported. In a numerical study, Wang and Jing [50] estimated the sound speed of the aberrator by the method introduced by Wydra *et al.* [77] and used the FMT to calculate the arrival times. Shapoori *et al.* [52] also estimated the sound speed of the aberrator by the method introduced by Wydra *et al.* [77] and used Fermat's principle for arrival time calculation, but no transcranial image through a human skull was reported. Wang and Jing [50] and Shapoori *et al.* [52] used focused transmit beams, which necessitates calculating and applying transmit delays for each image line; this imposes complexity to the imaging strategy. White and Venkatesh [6] reported on phase-corrected transcranial super resolution ultrasound imaging through the temporal region of human skull with a commercial probe, but the correction was achieved with a ground truth measurement, which is not feasible *in vivo*.

Other approaches rely on the injection of an ultrasound contrast agent. Contrast agent microbubbles can serve as bright point sources. Each bubble enables the estimation of a phase

Authorized licensed use limited to: TU Delft Library. Downloaded on April 25,2022 at 06:57:05 UTC from IEEE Xplore. Restrictions apply.

aberration correction for optimal image reconstruction in the area close to the bubble [16]. By repeating the procedure with multiple microbubbles located at different positions in the region of interest, it is possible to design multiple isoplanatic patches.

The proposed method in this article seems to address the abovementioned limitations. It does not require any prior information on the skull (geometry, position with respect to the probe, wave speed), nor injection of an ultrasound contrast agent. Our approach is simpler to implement because it is not iterative, it only uses one ultrasound array transducer and relies on the transmission of unfocused beams and synthetic focusing in transmit and receive, which makes it simpler in terms of programming the ultrasound scanner in transmit. While our method was used before for *in vivo* imaging of the inner structure of the radius and tibia bone [67], here we showed that it has the potential to correct images of the brain through the human temporal bone.

B. Limitations and Assumptions of the Proposed Approach

In our approach, the wave speed in the temporal bone was considered isotropic. While a more accurate velocity model could improve the performance of our phase correction technique [67], [79], limited information is unfortunately available on the anisotropy elastic properties of the temporal bone. As reported in [29], the wave speed exhibits a maximum value for a certain direction within the plane of the bone layer and minimum value (about 13% smaller) in a direction normal to the plane of the bone layer. Like in long bones, the autofocus method could be used in combination with the bidirectional headwave technique to estimate a model of anisotropic compressional sound speed in the temporal bone [67], [79], [94], and this will be considered in future work.

In addition, the temporal bone was described as a homogeneous layer of cortical bone in this study. Therefore, the approach would likely not perform well if the temporal bone contains cancellous bone (diploe) between two cortical bone layers. Because of this limitation, we do not expect our approach to significantly reduce the rate of TWF, since it is mainly caused by temporal bone heterogeneity. The skull used in our experiment was an easy case since its estimated thickness was 1.3 mm, which is a thin temporal bone compared with the thickness range of 1.5–2.9 mm reported in the literature [28]. In follow-up experiments, more skull specimens should be studied to investigate the robustness of our method. Note that at the time of writing, the availability of human skull specimens was limited. Recently, more specimens became available (see https://www.skullsunlimited.com/collections/all). Our approach may be further developed by describing the temporal bone with a three-layer model.

The near surface of the temporal window was assumed planar when estimating the wave speed in bone with the headwave method [59]–[61]. This can be a fair assumption considering the small footprint of the P4-1 probe (i.e., a lateral width of 28 mm). Yet, development of techniques to compensate for the bone curvature (in the lateral direction) and even bone irregularities could be of interest for a more accurate compressional sound speed estimation [95], [96].

The elevation effect of the 1-D array was ignored. For the velocity measurement in long bone, this effect is negligible [60] due to the nearly cylindrical shape of the diaphysis of a long bone. However, the geometry of the temporal bone is more complex. In addition, the possible change of imaging plane in the elevation direction in the presence of an aberrator could explain the higher localization errors in the experimental results, compared with numerical ones (see Table I). Like all aberration correction methods, the use of a matrix array would improve the performance of our approach. With a matrix array, the 3-D position and geometry of the temporal bone could be estimated with a strategy very similar to that proposed in this manuscript and travel times could be accurately calculated in a 3-D space.

To sum up, the anisotropy of the bone layer (wave speed depends on propagation direction), the skull microstructure (one-layer or three-layer bone), the 3-D geometry of the bone layer (transducer not being parallel with respect to the boundaries of the bone layer in the elevation direction), and the influence of superficial soft tissues should be taken into account for *in vivo* experiments.

C. Imaging Scheme and Implementation

1) Beamforming: Several approaches (for instance, Wang and Jing [50] and Shapoori *et al.* [52]) used focused transmit beams. Like [16], [56], our approach uses unfocused transmit beams and relies on a SAI sequence with single-element transmission. It allows 1) to calculate the trajectory of the wave (necessary for phase correction) and 2) to have dynamic focusing in both transmission and reception [57]. The latter provides a high image quality, which helps the segmentation of the near and far interfaces of the temporal bone and, therefore, the construction of an accurate SSM. A delay-and-sum beamformer was used to reconstruct the images. However, more advanced beamforming methods could improve the resolution, lower the level of background noise, and even reduce the effects of multiple reflections [97]–[104].

2) Computational Time: Our approach requires 8 s to estimate the arrival times, and 13 s to reconstruct a refraction-corrected image using data acquired by 96 elements (and therefore 96 single-element transmissions) with an Intel Core i7-8650U CPU, without any parallel computing. A real-time visualization is needed for *in vivo* applications. The processing complexity of our method is relatively low. Using a very similar strategy, a frame rate of four images per second was reported in [79] for imaging long bones. However, a relatively larger imaging depth is needed for brain imaging (the center of the circle of Willis is located at a depth of about 7 cm), which increases the computational time for reconstructing one frame. Further development of our technique with parallel computing on GPUs or CPUs might provide a fast enough reconstruction [105]–[108].

Authorized licensed use limited to: TU Delft Library. Downloaded on April 25,2022 at 06:57:05 UTC from IEEE Xplore. Restrictions apply.

D. Improving Cerebral Blood Flow Characterization With TUI and Frame Rate

As shown in [16], [33], [46], [47], aberration correction improves blood flow imaging with TUI in subjects without TWF. The improvement of spatial resolution and contrast also improves the detection of blood flow. Future work should investigate the added value of our approach for imaging blood flow in the cerebral arteries.

The frame rate of SAI sequence is limited to about 100 Hz (considering 96 elements for transmission, a depth of 7 cm [28], and a sound speed of 1500 m/s for the brain). This frame rate is sufficient for brain anatomical imaging, but not high enough for blood flow quantification in the brain [109]. Once the sonographer has found the best window on the temporal region of skull to image through using the synthetic aperture sequence, the correction method could be extended to a high frame rate mode, using the transmission of plane waves or diverging waves (with the concept of virtual point sources). This also ensures a good signal-to-noise ratio since all the array elements can be activated (with the appropriate transmit delays) for the transmission of a plane or diverging wave.

V. Conclusion

In this article, we introduced a technique to improve the correction of the refraction caused by the temporal bone in single-sided 2-D TUI using a commercial probe. The novelty lies in the fact that the position and true geometry of the bone layer and the wave speed in the cortical bone are estimated with a single ultrasound probe. First, the head wave was used for compressional sound velocity estimation. Then, SSMs were fed to the FMT for arrival time calculation. Finally, images were reconstructed through adaptive beamforming. The proposed approach substantially improved the image quality in experiments consisting of imaging a wire phantom placed behind a bone-mimicking plate or a human skull.

References

[1] T. Hölscher *et al.*, "Transcranial ultrasound from diagnosis to early stroke treatment," *Cerebrovascular Diseases*, vol. 26, no. 6, pp. 659–663, 2008.

[2] F. Schlachetzki *et al.*, "Transcranial ultrasound from diagnosis to early stroke treatment–Part 2: Prehospital neurosonography in patients with acute stroke–The regensburg stroke mobile project," *Cerebrovascular Diseases*, vol. 33, no. 3, pp. 262–271, 2012.

[3] T. Holscher, "Prehospital use of portable ultrasound for stroke diagnosis and treatment initiation," *Air Rescue*, vol. 2, pp. 48–50, Feb. 2012.

[4] D. Antipova, L. Eadie, S. Makin, H. Shannon, P. Wilson, and A. Macaden, "The use of transcranial ultrasound and clinical assessment to diagnose ischaemic stroke due to large vessel occlusion in remote and rural areas," *PLoS ONE*, vol. 15, no. 10, Oct. 2020, Art. no. e0239653.

[5] M. Herzberg *et al.*, "Prehospital stroke diagnostics based on neurological examination and transcranial ultrasound," *Crit. Ultrasound J.*, vol. 6, no. 1, pp. 1–13, Dec. 2014.

[6] H. White and B. Venkatesh, "Applications of transcranial Doppler in the ICU: A review," *Intensive Care Med.*, vol. 32, no. 7, pp. 981–994, 2006.

[7] D. W. Newell, S. M. Grady, J. M. Eskridge, and R. H. Winn, "Distribution of angiographic vasospasm after subarachnoid hemorrhage: Implications for diagnosis by transcranial Doppler ultrasonography," *Neurosurgery*, vol. 27, no. 4, pp. 574–577, Oct. 1990.

[8] Y. Y. Vora, M. Suarez-Almazor, D. E. Steinke, M. L. Martin, and J. M. Findlay, "Role of transcranial Doppler monitoring in the diagnosis of cerebral vasospasm after subarachnoid hemorrhage," *Neurosurgery*, vol. 44, no. 6, pp. 1237–1248, Jun. 1999.

[9] T. S. Padayachee, S. Parsons, R. Theobold, J. Linley, R. G. Gosling, and P. B. Deverall, "The detection of microemboli in the middle cerebral artery during cardiopulmonary bypass: A transcranial Doppler ultrasound investigation using membrane and bubble oxygenators," *Ann. Thoracic Surg.*, vol. 44, no. 3, pp. 298–302, Sep. 1987.

[10] D. C. Tong and G. W. Albers, "Transcranial Doppler–detected microemboli in patients with acute stroke," *Stroke*, vol. 26, no. 9, pp. 1588–1592, 1995.

[11] M. T. Graham, J. Huang, F. X. Creighton, and M. A. Lediju Bell, "Simulations and human cadaver head studies to identify optimal acoustic receiver locations for minimally invasive photoacoustic-guided neurosurgery," *Photoacoustics*, vol. 19, Sep. 2020, Art. no. 100183.

[12] M. A. L. Bell, A. K. Ostrowski, K. Li, P. Kazanzides, and E. M. Boctor, "Localization of transcranial targets for photoacoustic-guided endonasal surgeries," *Photoacoustics*, vol. 3, no. 2, pp. 78–87, 2015.

[13] M. A. L. Bell, A. K. Ostrowski, P. Kazanzides, and E. Boctor, "Feasibility of transcranial photoacoustic imaging for interventional guidance of endonasal surgeries," *Proc. SPIE*, vol. 8943, Mar. 2014, Art. no. 894307.

[14] D. E. Soulioti, D. Espindola, P. A. Dayton, and G. F. Pinton, "Super-resolution imaging through the human skull," *IEEE Trans. Ultrason., Ferroelectr., Freq. Control*, vol. 67, no. 1, pp. 25–36, Jan. 2020.

[15] C. Errico *et al.*, "Ultrafast ultrasound localization microscopy for deep super-resolution vascular imaging," *Nature*, vol. 527, no. 7579, pp. 499–502, Nov. 2015.

[16] C. Demené *et al.*, "Transcranial ultrafast ultrasound localization microscopy of brain vasculature in patients," *Nature Biomed. Eng.*, vol. 5, no. 3, pp. 219–228, Mar. 2021.

[17] E. Tiran *et al.*, "Transcranial functional ultrasound imaging in freely moving awake mice and anesthetized young rats without contrast agent," *Ultrasound Med. Biol.*, vol. 43, no. 8, pp. 1679–1689, 2017.

[18] J. Baranger *et al.*, "Bedside functional monitoring of the dynamic brain connectivity in human neonates," *Nature Commun.*, vol. 12, no. 1, pp. 1–10, Dec. 2021.

[19] M. Wiesmann and G. Seidel, "Ultrasound perfusion imaging of the human brain," *Stroke*, vol. 31, no. 10, pp. 2421–2425, Oct. 2000.

[20] L. Saba and E. Raz, *Neurovascular Imaging: From Basics to Advanced Concepts*. New York, NY, USA: Springer, 2016.

[21] V. I. Lau *et al.*, "Better with ultrasound: Transcranial Doppler," *Chest*, vol. 157, no. 1, pp. 142–150, 2020.

[22] J. D. Kirsch, M. Mathur, M. H. Johnson, G. Gowthaman, and L. M. Scoutt, "Advances in transcranial Doppler U.S.: Imaging ahead," *RadioGraphics*, vol. 33, no. 1, pp. E1–E14, Jan. 2013.

[23] F. J. Fry and J. E. Barger, "Acoustical properties of the human skull," *J. Acoust. Soc. Amer.*, vol. 63, no. 5, pp. 1576–1590, May 1978.

[24] F. Vignon, J.-F. Aubry, M. Tanter, A. Margoum, and M. Fink, "Adaptive focusing for transcranial ultrasound imaging using dual arrays," *J. Acoust. Soc. Amer.*, vol. 120, no. 5, pp. 2737–2745, Aug. 2015.

[25] G. Pinton, J.-F. Aubry, E. Bossy, M. Müller, M. Pernot, and M. Tanter, "Attenuation, scattering, and absorption of ultrasound in the skull bone," *Med. Phys.*, vol. 39, no. 1, pp. 299–307, Jan. 2012.

[26] F. Vignon, W. T. Shi, X. Yin, T. Hoelscher, and J. E. Powers, "The stripe artifact in transcranial ultrasound imaging," *J. Ultrasound Med.*, vol. 29, no. 12, pp. 1779–1786, Dec. 2010.

[27] R. T. Brisson *et al.*, "Association between tomographic characteristics of the temporal bone and transtemporal window quality on transcranial color Doppler ultrasound in patients with stroke or transient ischemic attack," *Ultrasound Med. Biol.*, vol. 47, no. 3, pp. 511–516, Mar. 2021.

[28] C.-H. Lee, S.-H. Jeon, S.-J. Wang, B.-S. Shin, and H. G. Kang, "Factors associated with temporal window failure in transcranial Doppler sonography," *Neurol. Sci.*, vol. 41, no. 11, pp. 3293–3299, Nov. 2020.

[29] J. Peterson and P. C. Dechow, "Material properties of the human cranial vault and zygoma," *Anatomical Rec.*, vol. 274A, no. 1, pp. 785–797, Sep. 2003.

[30] J.-H. Kwon, J. S. Kim, D.-W. Kang, K.-S. Bae, and S. U. Kwon, "The thickness and texture of temporal bone in brain CT predict acoustic window failure of transcranial Doppler," *J. Neuroimaging*, vol. 16, no. 4, pp. 347–352, Oct. 2006.

[31] A. Y. Ammi *et al.*, "Characterization of ultrasound propagation through *ex-vivo* human temporal bone," *Ultrasound Med. Biol.*, vol. 34, no. 10, pp. 1578–1589, Feb. 2008.

Authorized licensed use limited to: TU Delft Library. Downloaded on April 25,2022 at 06:57:05 UTC from IEEE Xplore. Restrictions apply.

[32] Z. Kardos *et al.*, "Increased frequency of temporal acoustic window failure in rheumatoid arthritis: A manifestation of altered bone metabolism?" *Clin. Rheumatol.*, vol. 37, no. 5, pp. 1183–1188, May 2018.

[33] B. D. Lindsey, H. A. Nicoletto, E. R. Bennett, D. T. Laskowitz, and S. W. Smith, "Simultaneous bilateral real-time 3-D transcranial ultrasound imaging at 1 MHz through poor acoustic Windows," *Ultrasound Med. Biol.*, vol. 39, no. 4, pp. 721–734, Apr. 2013.

[34] G. Seidel and S. Meairs, "Ultrasound contrast agents in ischemic stroke," *Cerebrovascular Diseases*, vol. 27, no. 2, pp. 25–39, 2009.

[35] G. Gahn *et al.*, "Contrast-enhanced transcranial color-coded duplex-sonography in stroke patients with limited bone windows," *Amer. J. Neuroradiol.*, vol. 21, no. 3, pp. 509–514, 2000.

[36] S. W. Smith, G. E. Trahey, and O. T. von Ramm, "Phased array ultrasound imaging through planar tissue layers," *Ultrasound Med. Biol.*, vol. 12, no. 3, pp. 229–243, Mar. 1986.

[37] S. Smith, O. Von Ramm, J. Kisslo, and F. Thurstone, "Real time ultrasound tomography of the adult brain," *Stroke*, vol. 9, no. 2, pp. 117–122, 1978.

[38] A. Kyriakou, E. Neufeld, B. Werner, M. M. Paulides, G. Szekely, and N. Kuster, "A review of numerical and experimental compensation techniques for skull-induced phase aberrations in transcranial focused ultrasound," *Int. J. Hyperthermia*, vol. 30, no. 1, pp. 36–46, 2014.

[39] S. Baykov *et al.*, "Physical and technical aspects of ultrasonic brain imaging through thick skull bones: 2. Experimental studies," *Acoust. Phys.*, vol. 49, no. 4, pp. 389–395, Jul. 2003.

[40] S. V. Baikov, A. M. Molotilov, and V. D. Svet, "Physical and technological aspects of ultrasonic imaging of brain structures through thick skull bones: 1. Theoretical and model studies," *Acoust. Phys.*, vol. 49, no. 3, pp. 276–284, May 2003.

[41] J. J. Dahl, M. S. Soo, and G. E. Trahey, "Spatial and temporal aberrator stability for real-time adaptive imaging," *IEEE Trans. Ultrason., Ferroelectr., Freq. Control*, vol. 52, no. 9, pp. 1504–1517, Sep. 2005.

[42] F. Vignon, J.-F. Aubry, M. Tanter, A. Margoum, M. Fink, and J. M. Lecoeur, "Dual-arrays brain imaging prototype: Experimental *in vitro* results," in *Proc. IEEE Ultrason. Symp.*, vol. 1, Sep. 2005, pp. 504–507.

[43] N. M. Ivancevich, J. J. Dahl, G. E. Trahey, and S. W. Smith, "Phase-aberration correction with a 3-D ultrasound scanner: Feasibility study," *IEEE Trans. Ultrason., Ferroelectr., Freq. Control*, vol. 53, no. 8, pp. 1432–1439, Aug. 2006.

[44] N. M. Ivancevich, G. F. Pinton, H. A. Nicoletto, E. Bennett, D. T. Laskowitz, and S. W. Smith, "Real-time 3-D contrast-enhanced transcranial ultrasound and aberration correction," *Ultrasound Med. Biol.*, vol. 34, no. 9, pp. 1387–1395, Sep. 2008.

[45] N. M. Ivancevich, J. J. Dahl, and S. W. Smith, "Comparison of 3-D multi-lag cross-correlation and speckle brightness aberration correction algorithms on static and moving targets," *IEEE Trans. Ultrason., Ferroelectr., Freq. Control*, vol. 56, no. 10, pp. 2157–2166, Oct. 2009.

[46] B. D. Lindsey and S. W. Smith, "Pitch-catch phase aberration correction for 3D ultrasound brain helmet," in *Proc. IEEE Int. Ultrason. Symp.*, Oct. 2011, pp. 2456–2459.

[47] B. D. Lindsey, H. A. Nicoletto, E. R. Bennett, D. T. Laskowitz, and S. W. Smith, "3-D transcranial ultrasound imaging with bilateral phase aberration correction of multiple isoplanatic patches: A pilot human study with microbubble contrast enhancement," *Ultrasound Med. Biol.*, vol. 40, no. 1, pp. 90–101, Jan. 2014.

[48] S. W. Smith *et al.*, "The ultrasound brain helmet: Feasibility study of multiple simultaneous 3D scans of cerebral vasculature," *Ultrasound Med. Biol.*, vol. 35, no. 2, pp. 329–338, 2009.

[49] B. D. Lindsey, E. D. Light, H. A. Nicoletto, E. R. Bennett, D. T. Laskowitz, and S. W. Smith, "The ultrasound brain helmet: New transducers and volume registration for *in vivo* simultaneous multi-transducer 3-D transcranial imaging," *IEEE Trans. Ultrason., Ferroelectr., Freq. Control*, vol. 58, no. 6, pp. 1189–1202, Jun. 2011.

[50] T. Wang and Y. Jing, "Transcranial ultrasound imaging with speed of sound-based phase correction: A numerical study," *Phys. Med. Biol.*, vol. 58, no. 19, p. 6663, 2013.

[51] X. Lin, M. Sun, Y. Liu, Z. Shen, Y. Shen, and N. Feng, "Variable speed of sound compensation in the linear-array photoacoustic tomography using a multi-stencils fast marching method," *Biomed. Signal Process. Control*, vol. 44, pp. 67–74, Jul. 2018.

[52] K. Shapoori, J. Sadler, A. Wydra, E. V. Malyarenko, A. N. Sinclair, and R. G. Maev, "An ultrasonic-adaptive beamforming method and its application for trans-skull imaging of certain types of head injuries; Part I: Transmission mode," *IEEE Trans. Biomed. Eng.*, vol. 62, no. 5, pp. 1253–1264, May 2015.

[53] C. Jiang *et al.*, "Ray theory-based transcranial phase correction for intracranial imaging: A phantom study," *IEEE Access*, vol. 7, pp. 163013–163021, 2019.

[54] Y. Jing, F. C. Meral, and G. T. Clement, "Time-reversal transcranial ultrasound beam focusing using a K-space method," *Phys. Med. Biol.*, vol. 57, no. 4, p. 901, 2012.

[55] G. Bouchoux *et al.*, "Experimental validation of a finite-difference model for the prediction of transcranial ultrasound fields based on CT images," *Phys. Med. Biol.*, vol. 57, no. 23, p. 8005, 2012.

[56] C. Jiang, Y. Li, K. Xu, and D. Ta, "Full-matrix phase shift migration method for transcranial ultrasonic imaging," *IEEE Trans. Ultrason., Ferroelectr., Freq. Control*, vol. 68, no. 1, pp. 72–83, Jan. 2021.

[57] J. A. Jensen, S. I. Nikolov, K. L. Gammelmark, and M. H. Pedersen, "Synthetic aperture ultrasound imaging," *Ultrasonics*, vol. 44, pp. e5–e15, Dec. 2006.

[58] B. D. Lindsey and S. W. Smith, "Refraction correction in 3D transcranial ultrasound imaging," *Ultrason. Imag.*, vol. 36, no. 1, pp. 35–54, 2014.

[59] E. Bossy, M. Talmant, and P. Laugier, "Effect of bone cortical thickness on velocity measurements using ultrasonic axial transmission: A 2D simulation study," *J. Acoust. Soc. Amer.*, vol. 112, no. 1, pp. 297–307, Jul. 2002.

[60] E. Bossy, M. Talmant, and P. Laugier, "Three-dimensional simulations of ultrasonic axial transmission velocity measurement on cortical bone models," *J. Acoust. Soc. Amer.*, vol. 115, no. 5, pp. 2314–2324, Apr. 2004.

[61] E. Bossy, M. Talmant, M. Defontaine, F. Patat, and P. Laugier, "Bidirectional axial transmission can improve accuracy and precision of ultrasonic velocity measurement in cortical bone: A validation on test materials," *IEEE Trans. Ultrason., Ferroelectr., Freq. Control*, vol. 51, no. 1, pp. 71–79, Jan. 2004.

[62] M. Mozaffarzadeh, C. Minonzio, N. de Jong, M. D. Verweij, S. Hemm, and V. Daeichin, "Lamb waves and adaptive beamforming for aberration correction in medical ultrasound imaging," *IEEE Trans. Ultrason., Ferroelectr., Freq. Control*, vol. 68, no. 1, pp. 84–91, Jan. 2021.

[63] M. Mozaffarzadeh *et al.*, "Erratum to 'Lamb waves and adaptive beamforming for aberration correction in medical ultrasound imaging,'" *IEEE Trans. Ultrason., Ferroelectr., Freq. Control*, vol. 68, no. 2, pp. 352–353, Feb. 2021.

[64] J. A. Sethian, *Level Set Methods and Fast Marching Methods: Evolving Interfaces in Computational Geometry, Fluid Mechanics, Computer Vision, and Materials Science*. Cambridge, U.K.: Cambridge Univ. Press, 1999.

[65] M. S. Hassouna and A. A. Farag, "Multistencils fast marching methods: A highly accurate solution to the Eikonal equation on Cartesian domains," *IEEE Trans. Pattern Anal. Mach. Intell.*, vol. 29, no. 9, pp. 1563–1574, Sep. 2007.

[66] D. Alleyne and P. Cawley, "A two-dimensional Fourier transform method for the measurement of propagating multimode signals," *J. Acoust. Soc. Amer.*, vol. 89, no. 3, pp. 1159–1168, May 1990.

[67] G. Renaud, P. Kruizinga, D. Cassereau, and P. Laugier, "*In vivo* ultrasound imaging of the bone cortex," *Phys. Med. Biol.*, vol. 63, no. 12, Jun. 2018, Art. no. 125010.

[68] H. Hasegawa and H. Kanai, "Effect of element directivity on adaptive beamforming applied to high-frame-rate ultrasound," *IEEE Trans. Ultrason., Ferroelectr., Freq. Control*, vol. 62, no. 3, pp. 511–523, Mar. 2015.

[69] M. Mozaffarzadeh *et al.*, "Receive/transmit aperture selection for 3D ultrasound imaging with a 2D matrix transducer," *Appl. Sci.*, vol. 10, no. 15, p. 5300, Jul. 2020.

[70] G. Renaud, J. L. Johnson, and D. Cassereau, "Real-time Kirchhoff migration for ultrasound imaging of the bone cortex," in *Proc. SEG Tech. Program Expanded Abstr.*, Aug. 2018, pp. 4797–4801.

[71] J. Shepherd, G. Renaud, P. Clouzet, and K. van Wijk, "Photoacoustic imaging through a cortical bone replica with anisotropic elasticity," *Appl. Phys. Lett.*, vol. 116, no. 24, Jun. 2020, Art. no. 243704.

[72] E. W. Dijkstra, "A note on two problems in connexion with graphs," *Numer. Math.*, vol. 1, no. 1, pp. 269–271, Dec. 1959.

[73] D. Hong, "Medical image segmentation based on accelerated Dijkstra algorithm," in *Advances in Intelligent Systems*. Berlin, Germany: Springer, 2012, pp. 341–348.

Authorized licensed use limited to: TU Delft Library. Downloaded on April 25,2022 at 06:57:05 UTC from IEEE Xplore. Restrictions apply.

[74] B. E. Treeby and B. T. Cox, "K-wave: MATLAB toolbox for the simulation and reconstruction of photoacoustic wave fields," *J. Biomed. Opt.*, vol. 15, no. 2, 2010, Art. no. 021314.
[75] G. Pinton, G. E. Trahey, and J. J. Dahl, "Sources of image degradation in fundamental and harmonic ultrasound imaging using nonlinear, full-wave simulations," *IEEE Trans. Ultrason., Ferroelectr., Freq. Control*, vol. 58, no. 4, pp. 754–765, Apr. 2011.
[76] J. Aarnio, G. T. Clement, and K. Hynynen, "A new ultrasound method for determining the acoustic phase shifts caused by the skull bone," *Ultrasound Med. Biol.*, vol. 31, no. 6, pp. 771–780, Jun. 2005.
[77] A. Wydra, E. Malyarenko, K. Shapoori, and R. G. Maev, "Development of a practical ultrasonic approach for simultaneous measurement of the thickness and the sound speed in human skull bones: A laboratory phantom study," *Phys. Med. Biol.*, vol. 58, no. 4, p. 1083, 2013.
[78] H. Nguyen Minh, J. Du, and K. Raum, "Estimation of thickness and speed of sound in cortical bone using multifocus pulse-echo ultrasound," *IEEE Trans. Ultrason., Ferroelectr., Freq. Control*, vol. 67, no. 3, pp. 568–579, Mar. 2020.
[79] G. Renaud, P. Clouzet, D. Cassereau, and M. Talmant, "Measuring anisotropy of elastic wave velocity with ultrasound imaging and an autofocus method: Application to cortical bone," *Phys. Med. Biol.*, vol. 65, no. 23, 2020, Art. no. 235016.
[80] L. Deng, A. Hughes, and K. Hynynen, "A noninvasive ultrasound resonance method for detecting skull induced phase shifts may provide a signal for adaptive focusing," *IEEE Trans. Biomed. Eng.*, vol. 67, no. 9, pp. 2628–2637, Sep. 2020.
[81] G. Clement, P. White, and K. Hynynen, "Enhanced ultrasound transmission through the human skull using shear mode conversion," *J. Acoust. Soc. Amer.*, vol. 115, no. 3, pp. 1356–1364, Mar. 2004.
[82] B. Lucht, A. Hubbell, and K. Hynynen, "Contrast-enhanced transcranial two-dimensional ultrasound imaging using shear-mode conversion at low frequency," *Ultrasound Med. Biol.*, vol. 39, no. 2, pp. 332–344, Feb. 2013.
[83] P. J. White, G. T. Clement, and K. Hynynen, "Longitudinal and shear mode ultrasound propagation in human skull bone," *Ultrasound Med. Biol.*, vol. 32, no. 7, pp. 1085–1096, Jul. 2006.
[84] A. Yousefi, D. E. Goertz, and K. Hynynen, "Transcranial shear-mode ultrasound: Assessment of imaging performance and excitation techniques," *IEEE Trans. Med. Imag.*, vol. 28, no. 5, pp. 763–774, May 2009.
[85] M. A. O'Reilly and K. Hynynen, "A super-resolution ultrasound method for brain vascular mapping," *Med. Phys.*, vol. 40, no. 11, 2013, Art. no. 110701.
[86] R. M. Jones *et al.*, "Echo-focusing in transcranial focused ultrasound thalamotomy for essential tremor: A feasibility study," *Movement Disorders*, vol. 35, no. 12, pp. 2327–2333, 2020.
[87] F. Vignon, W. T. Shi, M. R. Burcher, and J. E. Powers, "Determination of temporal bone isoplanatic patch sizes for transcranial phase aberration correction," in *Proc. IEEE Ultrason. Symp.*, Nov. 2008, pp. 1286–1289.
[88] K. A. Wear, "Autocorrelation and cepstral methods for measurement of tibial cortical thickness," *IEEE Trans. Ultrason., Ferroelectr., Freq. Control*, vol. 50, no. 6, pp. 655–660, Jun. 2003.
[89] J. Karjalainen, O. Riekkinen, J. Toyras, H. Kroger, and J. Jurvelin, "Ultrasonic assessment of cortical bone thickness *in vitro* and *in vivo*," *IEEE Trans. Ultrason., Ferroelectr., Freq. Control*, vol. 55, no. 10, pp. 2191–2197, Oct. 2008.
[90] T. Postert, J. Federlein, H. Przuntek, and T. Büttner, "Insufficient and absent acoustic temporal bone window: Potential and limitations of transcranial contrast-enhanced color-coded sonography and contrast-enhanced power-based sonography," *Ultrasound Med. Biol.*, vol. 23, no. 6, pp. 857–862, Jan. 1997.
[91] Q. Grimal and P. Laugier, "Quantitative ultrasound assessment of cortical bone properties beyond bone mineral density," *IRBM*, vol. 40, no. 1, pp. 16–24, Feb. 2019.
[92] L. Peralta, X. Cai, P. Laugier, and Q. Grimal, "A critical assessment of the *in-vitro* measurement of cortical bone stiffness with ultrasound," *Ultrasonics*, vol. 80, pp. 119–126, Sep. 2017.
[93] B. Martin and J. H. McElhaney, "The acoustic properties of human skull bone," *J. Biomed. Mater. Res.*, vol. 5, no. 4, pp. 325–333, Jul. 1971.
[94] B. E. Treeby, T. K. Varslot, E. Z. Zhang, J. G. Laufer, and P. C. Beard, "Automatic sound speed selection in photoacoustic image reconstruction using an autofocus approach," *J. Biomed. Opt.*, vol. 16, no. 9, 2011, Art. no. 090501.
[95] G. Lowet and G. Van der Perre, "Ultrasound velocity measurement in long bones: Measurement method and simulation of ultrasound wave propagation," *J. Biomechanics*, vol. 29, no. 10, pp. 1255–1262, Oct. 1996.
[96] I. Lerche, "On the reflection of acoustic waves from a slightly curved interface," *J. Acoust. Soc. Amer.*, vol. 81, no. 3, pp. 611–618, Mar. 1987.
[97] M. Mozaffarzadeh, A. Mahloojifar, M. Orooji, S. Adabi, and M. Nasiriavanaki, "Double-stage delay multiply and sum beamforming algorithm: Application to linear-array photoacoustic imaging," *IEEE Trans. Biomed. Eng.*, vol. 65, no. 1, pp. 31–42, Jan. 2018.
[98] M. Mozaffarzadeh, M. Sadeghi, A. Mahloojifar, and M. Orooji, "Double-stage delay multiply and sum beamforming algorithm applied to ultrasound medical imaging," *Ultrasound Med. Biol.*, vol. 44, no. 3, pp. 677–686, Mar. 2018.
[99] M. Mozaffarzadeh, A. Mahloojifar, M. Orooji, K. Kratkiewicz, S. Adabi, and M. Nasiriavanaki, "Linear-array photoacoustic imaging using minimum variance-based delay multiply and sum adaptive beamforming algorithm," *J. Biomed. Opt.*, vol. 23, no. 2, 2018, Art. no. 026002.
[100] G. Matrone, A. S. Savoia, G. Caliano, and G. Magenes, "The delay multiply and sum beamforming algorithm in ultrasound B-mode medical imaging," *IEEE Trans. Med. Imag.*, vol. 34, no. 4, pp. 940–949, Apr. 2015.
[101] G. Matrone, A. S. Savoia, G. Caliano, and G. Magenes, "Ultrasound synthetic aperture focusing with the delay multiply and sum beamforming algorithm," in *Proc. 37th Annu. Int. Conf. IEEE Eng. Med. Biol. Soc. (EMBC)*, Aug. 2015, pp. 137–140.
[102] J. Kang, D. Go, I. Song, and Y. Yoo, "Ultrafast power Doppler imaging using frame-multiply-and-sum-based nonlinear compounding," *IEEE Trans. Ultrason., Ferroelectr., Freq. Control*, vol. 68, no. 3, pp. 453–464, Mar. 2021.
[103] M. A. Lediju, G. E. Trahey, B. C. Byram, and J. J. Dahl, "Short-lag spatial coherence of backscattered echoes: Imaging characteristics," *IEEE Trans. Ultrason., Ferroelectr., Freq. Control*, vol. 58, no. 7, pp. 1377–1388, Jul. 2011.
[104] F. Vignon *et al.*, "The Stokes relations linking time reversal and the inverse filter," *J. Acoust. Soc. Amer.*, vol. 119, no. 3, pp. 1335–1346, Mar. 2006.
[105] S. R. Miri Rostami, M. Mozaffarzadeh, M. Ghaffari-Miab, A. Hariri, and J. Jokerst, "GPU-accelerated double-stage delay-multiply-and-sum algorithm for fast photoacoustic tomography using LED excitation and linear arrays," *Ultrason. Imag.*, vol. 41, no. 5, pp. 301–316, Sep. 2019.
[106] E. A. Gonzalez and M. A. L. Bell, "GPU implementation of photoacoustic short-lag spatial coherence imaging for improved image-guided interventions," *J. Biomed. Opt.*, vol. 25, no. 7, 2020, Art. no. 077002.
[107] D. Hyun, G. E. Trahey, and J. J. Dahl, "*In vivo* demonstration of a real-time simultaneous B-mode/spatial coherence GPU-based beamformer," in *Proc. IEEE Int. Ultrason. Symp. (IUS)*, Jul. 2013, pp. 1280–1283.
[108] B. Y. S. Yiu, I. K. H. Tsang, and A. C. H. Yu, "GPU-based beamformer: Fast realization of plane wave compounding and synthetic aperture imaging," *IEEE Trans. Ultrason., Ferroelectr., Freq. Control*, vol. 58, no. 8, pp. 1698–1705, Aug. 2011.
[109] C. Robba and G. Citerio, *Echography and Doppler of the Brain*. Switzerland: Springer, 2021. [Online]. Available: https://link.springer.com/book/10.1007/978-3-030-48202-2#about

Moein Mozaffarzadeh (Graduate Student Member, IEEE) received the B.Sc. degree in electrical engineering from the Babol Noshirvani University of Technology, Mazandaran, Iran, in 2015, and the M.Sc. degree in biomedical-bioelectric engineering from Tarbiat Modares University, Tehran, Iran, in 2017. He is currently pursuing the Ph.D. degree with the Laboratory of Medical Imaging, Department of Imaging Physics, Delft University of Technology, Delft, The Netherlands.

His research interests include photoacoustic/ultrasound imaging, acoustic beamforming, and medical ultrasound transducer design.

Authorized licensed use limited to: TU Delft Library. Downloaded on April 25,2022 at 06:57:05 UTC from IEEE Xplore. Restrictions apply.

Eric Verschuur (also known as Dirk J. Verschuur) received the M.Sc. and Ph.D. degrees (Hons.) in applied physics from the Delft University of Technology (DUT), Delft, The Netherlands, in 1986 and 1991, respectively.

Currently, he is an Associate Professor with the DUT within the Imaging Physics Department. Since 2016, he has been the Program Director of the Delphi Research Consortium, within which research is carried in the area of Geo-Imaging. His main research interests include wavefield modeling, data processing, imaging and inversion techniques, and the use of machine learning for geo-imaging.

Dr. Verschuur received SEG's J. Clarence Karcher Award in 1997 and he was awarded with the Virgil Kauffman Gold Medal from the SEG in 2006.

Martin D. Verweij (Member, IEEE) received the M.Sc. *(cum laude)* and Ph.D. degrees in electrical engineering from the Delft University of Technology, Delft, The Netherlands, in 1988 and 1992, respectively.

From 1993 to 1997, he was a Research Fellow with the Prestigious Royal Netherlands Academy of Arts and Sciences, Amsterdam, The Netherlands. In 1995 and 1997, he was a Visiting Scientist at Schlumberger Cambridge Research, Cambridge, U.K. In 1998, he became an Assistant Professor, and later an Associate Professor, with the Laboratory of Electromagnetic Research, Delft University of Technology, where he switched to the Laboratory of Acoustical Wavefield Imaging in 2011. Since 2015, he also has a part-time position at the Biomedical Engineering Group, Erasmus Medical Centre, Rotterdam, The Netherlands. He is a Research Leader of the Dutch Technology Foundation (STW) on projects involving transducer design, beamforming, and imaging. He was elected as the Best Teacher of the Electrical Engineering Curriculum in the academic year from 2001 to 2002. His research interests include dedicated transducer design, beamforming algorithms, and the theoretical modeling and numerical simulation of medical ultrasound. He is the originator of the iterative nonlinear contrast source method for the computation of nonlinear ultrasound fields.

Dr. Verweij is an Associate Editor of the *Journal of the Acoustical Society of America* and a Treasurer of the Dutch Society for Medical Ultrasound.

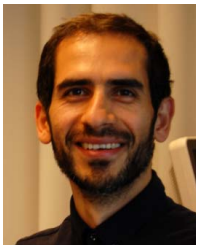

Verya Daeichin (Member, IEEE) received the Ph.D. degree in biomedical engineering from the Erasmus Medical Center, Rotterdam, The Netherlands, in 2015.

He was a Post-Doctoral Researcher with the Erasmus Medical Centre, where he focused on intravascular photoacoustic imaging for 18 months. Since 2016, he has been with the Medical Imaging Group, Delft University of Technology, Delft, The Netherlands. He is involved in running various medical ultrasound projects, focusing on novel multimodal ultrasound imaging. In 2019, he was a Visiting Scientist at the Laboratory of Prof. Mark Borden, University of Boulder, CO, USA, for five months, where he developed a novel photoacoustic-based microbubble characterization technique. His research interests include integrated bio-signal and ultrasound imaging, and ultrasound contrast agent.

Nico de Jong (Member, IEEE) received the degree from the Delft University of Technology, Delft, The Netherlands, in 1978. He received the M.Sc. degree in physics (specialized in the field of pattern recognition) from the Delft University of Technology, and the Ph.D. degree from the Erasmus Medical Center, Rotterdam, The Netherlands, in 1993. His Ph.D. dissertation was on acoustic properties of ultrasound contrast agents.

Since 1980, he has been a Staff Member at the Thorax Center, Erasmus Medical Center. In 2003, he was a part-time Professor at the Physics of Fluids Group, University of Twente, Enschede, The Netherlands. He teaches on technical universities and the Erasmus Medical Center. He has been a Promotor of 35 Ph.D. students and is currently supervising 11 Ph.D. students. Since 2011, he has been a Professor in molecular ultrasonic imaging and therapy with the Erasmus Medical Center and Delft University of Technology.

Dr. de Jong is the Organizer of the Annual European Symposium on Ultrasound Contrast Imaging, held in Rotterdam and attended by approximately 175 scientists from universities and industries all over the world. He is on the safety committee of the World Federation of Ultrasound in Medicine and Biology. Over the last five years, he has given more than 30 invited lectures and has given numerous scientific presentations for international industries. He has been a guest editor for special issues of different journals. He is an Associate Editor of *Ultrasound in Medicine and Biology*.

Guillaume Renaud received the Engineering degree from ICAM, Nantes, France, in 2004, the master's degree in acoustical physics from the University of Le Mans, Le Mans, France, in 2005, and the Ph.D. degree in biomedical physics from the University of Tours, Tour, France, in 2008.

After a post-doctoral fellowship at Erasmus MC, Rotterdam, The Netherlands, he was hired as a Tenured Scientist at CNRS, France, based within the Laboratory of Biomedical Imaging, Paris. His current research interests include nonlinear acoustics, imaging, and quantification of intraosseous blood flow and bone tissue properties with ultrasound.

Authorized licensed use limited to: TU Delft Library. Downloaded on April 25,2022 at 06:57:05 UTC from IEEE Xplore. Restrictions apply.